Trio: Utilizing Tag Interference for Refined Localization of Passive RFID

Han Ding*, Jinsong Han*†, Chen Qian‡, Fu Xiao§, Ge Wang*, Nan Yang*, Wei Xi*, and Jian Xiao¶
*School of Electronic and Information Engineering, Xi'an Jiaotong University, China
†Shaanxi Province Key Laboratory of Computer Network, Xi'an Jiaotong University, China
‡Department of Computer Engineering, University of California, Santa Cruz, USA
§College of Computer, Nanjing University of Posts and Telecommunications, China
¶Department of Electronic Science and Technology, Chang'an University, China

***Abstract*—We study a new problem, refined localization, in this paper. Refined localization calculates the location of an object in high precision, given that the object is in a relatively small region such as the surface of a table. Refined localization is useful in many cyber-physical systems such as industrial autonomous robots. Existing vision-based approaches suffer from several disadvantages, including good lighting conditions, line of sight, pre-learning process, and high computation overhead. Also vision-based approaches cannot differentiate objects with similar colors and shapes. This paper presents a new refined localization system, called Trio, which uses passive Radio Frequency Identification (RFID) tags for low cost and easy deployment. Trio provides a new angle to utilize RF interference for tag localization by modeling the equivalent circuits of coupled tags. We implement our prototype using commercial off-the-shelf RFID reader and tags. Extensive experiment results demonstrate that Trio effectively achieves high accuracy of refined localization, *i.e.*, < 1 cm errors for several types of main stream tags.**

I. Introduction

Object localization is of great importance for various applications and a lot of research activities have been conducted in this area. This work studies the *refined localization* problem: Given a number of objects in a (relatively small) region, such as the surface of a table or space in a shelf, refined localization calculates the location of each object in the region in high precision. Refined localization is useful in many cyber-physical systems such as autonomous robots. An industrial robot arm may need to perform precise motions, such as grasping, lifting, or carrying objects, within their working space [1]. A robot needs to know which objects are its targets and where they are, and then perform the manipulation tasks.

Existing approaches for refined localization mainly depend on computer vision techniques [2][3]. They usually employ visual sensors [4] to acquire high-resolution location information about the target objects. Using visual sensors, however, requires good lighting conditions and line of sight. Failures would occur if the environment is dim or the light-of-sight path from the sensor to the target is blocked. In addition, computer vision techniques need to learn the visual models of target objects in advance and may fail in detecting or recognizing objects with similar colors or shapes. Considering that massive similar objects are quite common in practice, such as in supermarkets, warehouses, libraries, *etc.*, computer vision techniques are insufficient for explicitly locating individual objects.

On the other hand, Radio Frequency (RF) based solutions are promising alternatives because they are cost-efficient and have little requirement of the environment or the line-of-sight constraint. Recently, researchers have developed a large body of works utilizing wireless signals, such as WiFi, RF radio, or acoustic signals, for navigation and localization [5][6][7][8]. Among existing IoT devices, Radio Frequency IDentificaiton (RFID) tags, especially the Ultra High Frequency (UHF) passive tags, are attractive for labeling a large amount of items and objectives, because they are cheap and battery-free. Localization of passive tags are challenging. The main difficulty is that one needs to create some relative movements between the reader and tags to generate physical signal changes, from which we can extract the distance and location information. Most prior solutions require special hardware that increases financial cost and deployment difficulty. For example, existing approaches may use synthetic aperture radar (SAR) or software-defined radios (SDR) to localize passive tags. Tagoram [9] uses multiple antennas deployed at the corners of a small region to localize a moving tag in the region. RF-Compass [10] utilizes a sliding antenna to simulate SAR for supporting robot navigation and object manipulation. Obviously, the movement of readers or target tags with strict average-speed limits a severe, sometimes impossible, hardware constraint in practice. More importantly, they were not designed for refined localization hence their accuracy may not satisfy the application requirements.

In this paper, we propose a *light-weight* and *cost-efficient* UHF RFID-based solution, namely Trio, for accurate refined localization. We study both the absolute localization, for which Trio reports the physical location of an object in a region, and relative localization, for which Trio reports the order of a number of objects in a region. The core idea in Trio is that it uses a pair of moving tags as reference tags. When the reference tags move close to a target tag, the three tags will cause special interference and physical signal changes. Compared to existing solutions, the two reference tags only cost several cents, significantly reducing the hardware cost. Trio is fully implemented with commodity off-the-shelf (COTS) UHF passive RFID devices. More importantly, it follows *the extensible RFID model* [11], [12], [13], [14], [15], [16], where the RFID reader used for Trio can be reused for other applications such as ordinary tracking and identification of

978-1-5386-4128-6/18/$31.00 ©2018 IEEE

items. It is because Trio only uses a limited capacity of a reader. Hence it can be easily deployed with existing RFID system and further reduces hardware cost and deployment difficulty.

We take autonomous robot arms as a typical application scenario for Trio. In our system, the manipulator is equipped with two passive tags (termed as the *reference pair* in the following). Trio detects and localizes the objects in a region with sub-centimeter level accuracy by moving the the reference pair (via manipulator) around the region. In this detection, the reference pair affects the electric fields of the tag attached to the target, implicitly changing its antenna structure and yielding variation of its scattering power (*e.g.*, a sharp decrease on its RSS). Thus, by analyzing the RSS variation, Trio can determine the location of the target tags. Furthermore, together with the temporal information Trio can also determine the order of a number of target objects along a direction.

We build a prototype of Trio using a COTS RFID reader (*i.e.*, Impinj R220), one directional patch antenna (*i.e.*, Laird A9028), and a number of passive tags (including 'Square', 'Short', 'Squiggle', 'Doc', 'Spider-360', 'BAT', and 'Impinj E41B'). Our results demonstrate that Trio can ultimately achieve < 1 cm localization accuracy for many main stream tags. Note that Trio can nicely complement vision-based localization methods. One big problem of vision-based methods is that they can hardly identify items with same shape and colors. RFID tags can easily provide the identity information. Locations can bridge the identities and visual objects.

II. System overview

Trio is an RFID-based object detection and refined localization solution. In Trio, we attach two UHF passive tags (*i.e.*, reference pair) to the manipulator, and one tag to each object. We assume that the tags on the manipulator and objects are all within the reading range of an RFID reader. The reader continuously interrogates all tags and reports their IDs, and the information of their signals, *e.g.*, Received Signal Strength (RSS). Based on the reported signal information, Trio enables two localization tasks: computing the location of an individual object (called absolute localization) and determining the order of objects along a direction (called relative localization).

The rationale behind Trio is the interaction among coupled tags, caused by the mutual coupling effects among closely-spaced linear antennas. According to this basis, the antenna structure of a target tag will change when the robot manipulator (*i.e.*, reference pair) is around it, resulting in a significant decrease on its scattering power and RSS. Leveraging this phenomenon, Trio moves along the horizontal and vertical direction respectively to estimate the target tag's location in the 2D plane (x-z plane), as shown in Fig. 1. On the other hand, to derive the order of objects in the array, we incorporate the time-domain information. By moving the reference pair in two dimensions and observing the sequence of tags in terms of their sharp RSS decreases, Trio can obtain the order of tags in each direction.

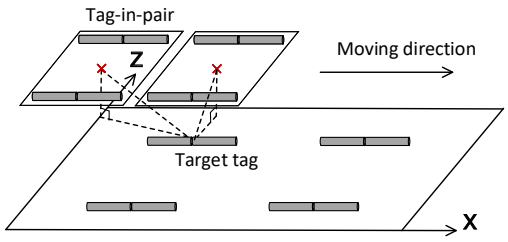

Fig. 1. Illustration of Trio design.

III. Modelling Tag Coupling in Trio

To understand the RF interference among tags caused by coupling, we first introduce the tag antenna design and antenna equivalent circuit. We then model the interference and analyze the radiation patten of coupled tags.

A. Tag Antenna Model

The antenna design of a UHF passive tag is correlated to the frequency at which the tag operates and the way it talks to the RFID reader. UHF tags utilize the *backscatter coupling* technique to reflect energy back to the reader antenna. Note that in this process, tags modulate some information (*i.e.*, ID) in the backscattered signal. Typically, they adopt the half-wave dipole-shaped antenna design.

The wavelength associated for UHF tags is about: $\lambda = c/f = \frac{3*10^8 m/s}{900MHz} \approx 32\ cm$, which means the half dipole antenna of each tag should be 16 cm long. Such a long antenna is obviously impractical for tags to be implemented in real applications. To tackle this problem, the wires of tag's antenna are usually bent, which is known as *meandered dipole*. A *Meander* of a half-wavelength dipole is able to fit on a typical printer label (say 10 cm), as the example (*e.g.*, Alien 964X) shown in Fig. 2(a).

In the meandered wire, the current flows in opposite directions in neighboring arms (Fig. 2(b)). These currents cancel with each other and contribute no radiation. Thus, only the segments along the original direction of the dipole generate radiating power. Hence, we can still treat the meander as an approximation of center-driven linear dipole.

B. Equivalent Circuit of a Tag

In order to further analyze tag radiation, we construct an *equivalent circuit* of a tag. A tag antenna is responsible of storing charge (*capacitance*), opposing changes in current (*inductance*), and radiating power out (*resistance*). As shown in Fig. 3(a), we can treat the tag antenna as a simplified electric circuit. In this circuit, a voltage source V_o connects a complex impedance (consisting a radiation resistance R_{rad} and a reactance X_{ant}, due to inductance, capacitance, or both) [17]. The IC can be similarly approximated as a linear and complex impedance ($Z_{IC} = R_{load} + jX_{IC}$). Here V_o is an open-circuit voltage, *i.e.*, the direct-current (DC) power arising from the incoming RF signal of the reader, which is theoretically derived from Frris function (correlating to the reader transmitting power, reader-to-tag distance, reader antenna gain, *etc.*) and remains constant for the tag in a static system.

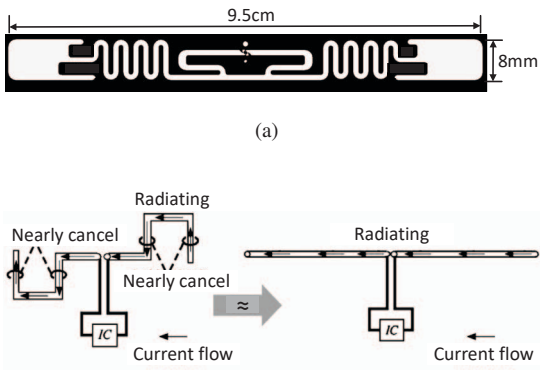

Fig. 2. (a) Meandered structure of the tag. (b) Only the current in segments along the original dipole direction of a meandered structure radiates.

In above circuit, the current flows through the resistors can be expressed via Ohm's law:

$$I = \frac{V_o}{(R_{rad} + jX_{ant}) + (R_{load} + jX_{IC})} = \frac{V_o}{Z_{ant} + Z_{IC}} \quad (1)$$

Then, the power delivered to IC is:

$$P_{load} = \frac{|I|^2 R_{load}}{2} = \frac{V_o^2 R_{load}}{2|Z_{ant} + Z_{IC}|^2} \quad (2)$$

The design principle of commodity UHF passive tag's antenna is to deliver enough power to the tag's IC for activation. According to Eq. 2, it is obvious that for fixed load and antenna resistors, the largest power will be obtained when the above denominator is minimized, that is, when the reactance X_{ant} and X_{IC} cancel each other. In this case, the circuit can be simplified as the one illustrated in Fig. 3(b). Furthermore, to figure out the relationship between R_{load} and R_{rad}, we divide the numerator and denominator of P_{load} by R_{rad}^2 concurrently:

$$P_{load} = \frac{V_o^2 R_{load}}{2(R_{rad} + R_{load})^2} = \frac{1}{R_{rad}} \cdot \frac{V_o^2 (R_{load}/R_{rad})}{2[1 + (R_{load}/R_{rad})]^2} \quad (3)$$

According to Eq. 3, we plot the relation between the ratio of R_{load} to R_{rad} and the IC power in Fig. 4, where V_o is set to 1. The figure indicates that with fixed R_{rad}, IC will obtain the maximum power when the load and radiation resistance are equal, which is the commonly used design of tag circuits. Generally, if the real parts of antenna and IC impedance are the same, and the imaginary parts only differ in the sign, the two impedances are called *conjugate matching*. For a matched antenna design, the tag will backscatter as much power as that is delivered to the IC and achieve the best efficiency.

For real tags, we may assume that their antennas are all designed to be *matched* to the IC. That is, the antenna and IC are adjusted so that the power possibly delivered to the IC is maximized. In this case, the corresponding scattered power of an individual tag is:

$$P_{rad} = P_{load} = \frac{V_o^2}{8R_{rad}} \quad (4)$$

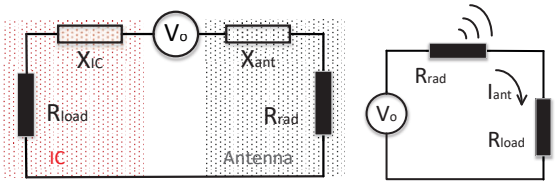

Fig. 3. (a) Equivalent circuit of the tag. (b) Conjugate-matched Case.

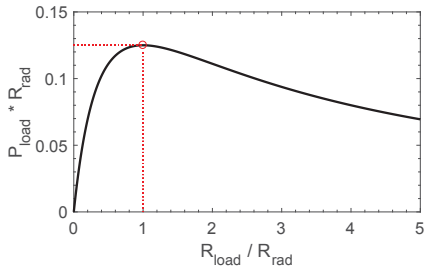

Fig. 4. The relationship between the obtained IC power and the ratio of the load to radiation resistance.

C. Model of Tag Coupling

For a certain tag, the impedance of IC ($Z_{IC} = R_{load} + jX_{IC}$) is fixed after the manufacture, which indicates that Eq. 4 is constant. However, when two or more tags are placed close to one another, mutual coupling effects will implicitly change the structure of the tag antenna, breaking the aforementioned *matched* condition. That is, the antenna impedance and backscattered power will both change, which can be leveraged for sensing the event of approaching certain tags. Therefore, we are inspired to investigate the mutual coupling among tags.

Mutual impedance is a general measure on the proximity effects of mutual coupling [18]. Consider two parallel linear dipoles of two tags, as shown in Fig. 5. Their distance along the x-axis is d, and their centers are offset to each other by b along the z-axis. The near field generated by the current on Tag 2 will induce a voltage on tag 1, which will produce the mutual impedance (Z_{21}) to tag 1:

$$Z_{21} = \frac{-1}{I_1 I_2} \int_{-h_2}^{h_2} E_{21}(z) I_2(z) dz = \frac{j\eta}{4\pi \sin kh_1 \sin kh_2 \int_{-h_2}^{h_2} F(z) dz}$$

$$where$$

$$\begin{cases} F(z) = [\dfrac{e^{-jkR_1}}{R_1} + \dfrac{e^{-jkR_2}}{R_2} - 2\cos kh_1 \dfrac{e^{-jkR_0}}{R_0}] \sin(k(h_2 - |z|)) \\ h_1 = l_1/2, \ h_2 = l_2/2 \end{cases} \quad (5)$$

Details of the derivation process can be referred in [19]. In fact, when there is only one tag in the region of interests (*i.e.*, the *target tag*), the radiation impedance Z_{ant} in Eq. 2 is actually the self impedance (Z_{11}) of the tag's antenna, which can also be calculated by Eq. 5.

Assuming that several (N) identical parallel dipoles are located near the target tag. In this case, mutual impedance will

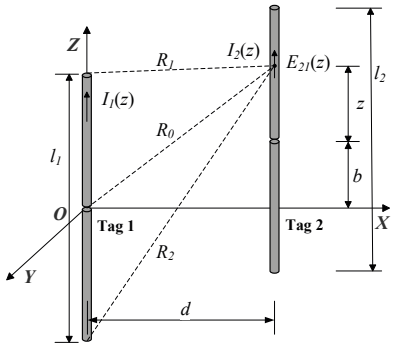

Fig. 5. Parallel dipoles.

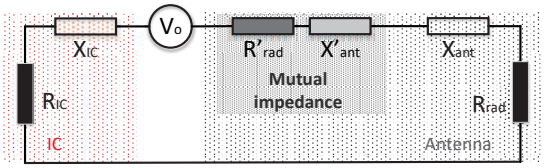

Fig. 6. Revised equivalent circuit of the target tag with coupled tags around.

occur, producing a virtual circuit as shown in Fig. 6. Then, the integrated impedance on the target tag's antenna will be:

$$Z_{rad'} = Z_{rad} + \sum_{i=1}^{N} Z_{i1} \tag{6}$$

where $Z_{i1} = R_{i1} + jX_{i1}$ is the mutual impedance caused by tag i. In Fig. 6, let ${R_{rad}}' = \sum_{i=1}^{N} R_{i1}$, ${X_{rad}}' = \sum_{i=1}^{N} X_{i1}$. Compared to Eq. 4, the scatter power newly yielded in this case is:

$$\begin{aligned} \tilde{P_{rad}} &= \frac{V_o^2({R_{rad}} + {R_{rad}}')}{2|{Z_{ant}} + Z_{IC} + {R_{rad}}' + {X_{ant}}'|^2} \\ &= \frac{V_o^2({R_{rad}} + {R_{rad}}')}{2|2{R_{rad}} + {R_{rad}}' + {X_{ant}}'|^2} \end{aligned} \tag{7}$$

Given above analysis along with Eq. 4, Eq. 5, and Eq. 7, we can model the backscatter power of the target tag under the situations with and without interfering tags around it, respectively. We build the coordinate system as illustrated in Fig. 7, where the target tag (Tag 1) locates at the origin of coordinates. I is the midpoint of the reference pair (*i.e.*, Tag 2 and 3). Then we change the location of reference pair in parallel with the x-z plane to test the scatter power of the target tag. The distance between two interfering tags along the x-axis is set to $d_{23} = 0.25\lambda$, and we have the corresponding position relation during the movement:

$$\begin{aligned} d_{12} &= \sqrt{(x_2 - x_1)^2 + (y_2 - y_1)^2} \\ d_{13} &= \sqrt{(x_3 - x_1)^2 + (y_3 - y_1)^2} \\ b &= |z_2 - z_1| = |z_3 - z_1| \end{aligned} \tag{8}$$

where,

$$\begin{cases} x = |x_3 - x_2|/2, \ y = y_2 = y_3, \ z = z_2 = z_3 \\ x_3 = |x_2 - d_{23}| \end{cases}$$

Fig. 8 compares the power of target tag when one and two interfering tags are located at different positions around it.

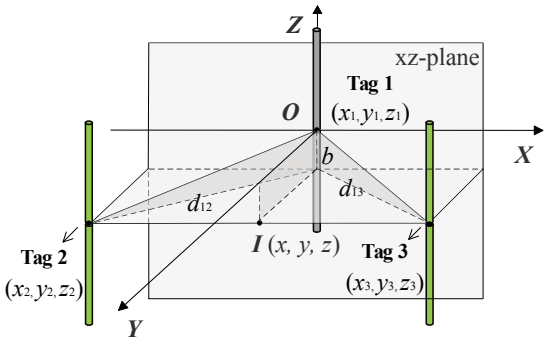

Fig. 7. Illustration of the coordinate system of Trio-based scheme.

Note that the gray plane is the *power* value of the individual target tag at origin O; the x and b values in the two-interfering-tags case are the coordinates of midpoint I. Fig. 8 implies that Trio demonstrates attractive advantages in sensing the target tag. We have the following insights: (1) Compared to one-interfering-tag case, at each height (*i.e.*, distance along the y-axis), Trio always has larger mutual impedance, producing larger power decrease when the reference pair are near the target tag. (2) When the height approaches to the wavelength, the mutual coupling derived from interfering tag/tags becomes negligible. (3) The closer the reference pair is, the larger power decrease the target tag will experience. Above insights inspire us that we could observe the RF interference among coupled tags to get the relative position of the target corresponding to the reference pair and localize the target tag.

To verify the effectiveness of above model, we conduct a proof-the-concept experiment. We deploy the target tag on a table (in the x-z plane), and put the reference pair in the same plane. We vary the z and x coordinates for the reference pair (the height is constant, *e.g.*, $y \approx 0$). The reader antenna is mounted on the ceiling, illuminating tags on the table. Fig. 9(b) shows the real Received Signal Strength (RSS) values of the target tag, while Fig. 9(a) plots the theoretical RSS deduced from our model. Note that the RSS reported by the Commercial off-the-shelf reader (Impinj Speedway Revolution R420) is measured in the unit of dBm. $\tilde{P_{rad}}$ of Eq. 7 can be converted to RSS by:

$$\tilde{RSS_{rad}} = 10 \cdot \log_{10}(1000 \cdot \tilde{P_{rad}}/1W) \tag{9}$$

From the figure, we can see that the real RSS distribution is almost consistent to the model. The figure demonstrates the substantial influence of coupled tags. Combining our prior analysis, the result reveals that *by observing the RSS valley of the target tag, it is possible to infer its position with respect to the reference pair.*

IV. Trio-based Localization

After confirming the feasibility of Trio in tag localization, we deploy the reference pair as interfering tags to perform both the absolute and relative localization tasks. Note that Trio is designed for accurate refined localization, the navigation of the robot to the proximity of targets could be realized by existing approaches of long-range coarse-grained localization [20].

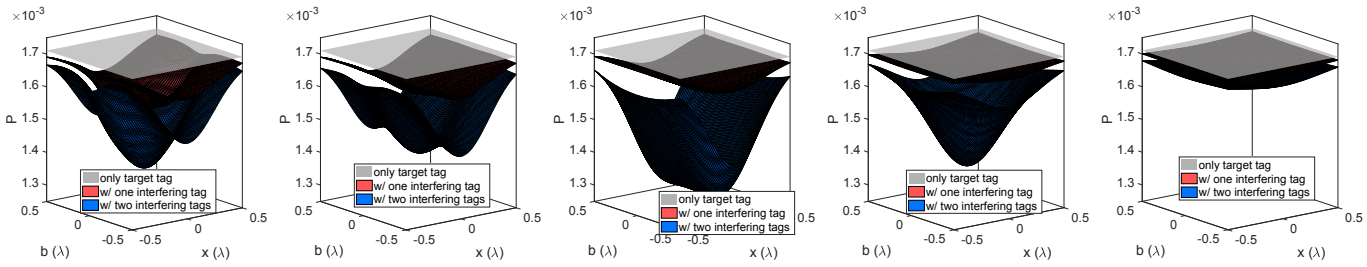

(a) height = 0.01λ (b) height = 0.25λ (c) height = 0.5λ (d) height = 0.75λ (e) height = 1λ

Fig. 8. Power spectrum from theoretical model.

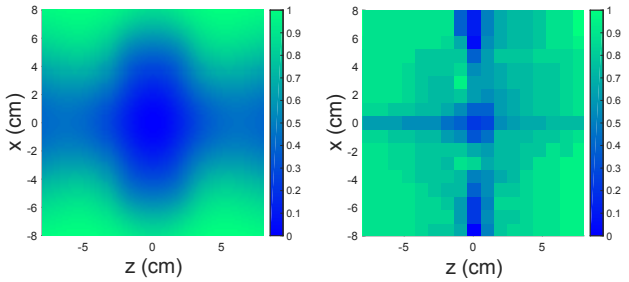

(a) (b)

Fig. 9. RSS distribution with one reference pair locating at different positions in the x-z plane. (a) simulation results derived from the theoretical model (b) RSS collected from real measurements.

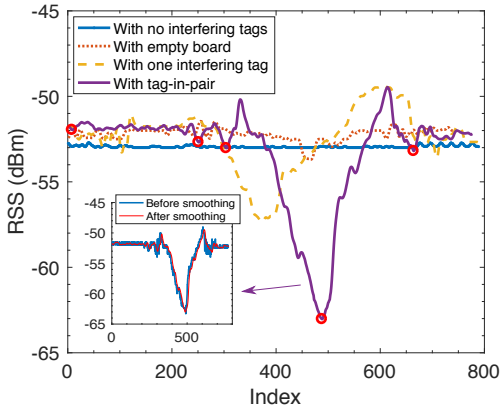

Fig. 10. RSS trends of the target tag under different situations.

A. Trio-based absolute localization

When the manipulator moves around the target tag, we track the RSS variation of the target tag to estimate its location: theoretically, the target tag reports its minimum RSS value when it locates exactly at the midpoint of two interfering tags. To achieve better efficiency and reliability, the absolute localization algorithm of Trio comprises of three modules, data preprocessing, valley detection, and iterative location refining.

1) Data preprocessing: This process is to smooth the RSS measurements and mitigate the noise. Each commodity reader has its minimum measurable change in RSS (*i.e.*, the resolution). For example, the Impinj reader adopted in Trio is about 0.5 dBm. Such a resolution could generate jitters or local discontinuity in the reported RSS values. In addition, environmental factors, such as multipath propagation, may also introduce noises to the RSS measurement. We thereby apply a triangular moving average filter to smooth the RSS data. The sub-figure in Fig. 10 shows the RSS measurements of target tag before/after performing the smoothing process. The slight difference between two curves demonstrate that the filter effectively enhances the stability and continuity of RSS measurements yet clearly captures the primary variations.

2) Automatic multiscale-based valley detection: As aforementioned, the valley in an RSS curve is an essential feature to fetch the accurate location of the tag. Thus, the second module of absolute localization in Trio is to detect the valley along the target tag's RSS curve. Considering that in real applications the reported RSS usually has certain amount of noise, we use the automatic multi-scale based peak detection (AMPD) method [21] to identify the peak (valley) value. Proved to be effective, AMPD is usually used for automatic detection on the peaks in noisy quasi-periodic signals.

The RSS values in the time series can be denoted as:

$$R = \{RSS_1, RSS_2, ..., RSS_N\} \tag{10}$$

Then the peak is detected by finding which $\sigma_i = 0$ holds in all possible indices $i \in [1, N]$ [21]:

$$\sigma_i = \frac{1}{\gamma - 1}\Sigma_{k=1}^{\gamma}[(m_{k,i} - \frac{1}{\gamma}\Sigma_{k=1}^{\gamma}m_{k,i})^2]^{\frac{1}{2}}, i = 1, 2, ..., N \tag{11}$$

where γ represents the scale with the most local maxima, and $m_{k,i}$ corresponds to the local maxima scalogram (LMS) of signal RSS. Note that in the real implementation, we use the absolute value of RSS stream as the input of AMPD algorithm to get the indexes of peaks, which correlates to the desired valleys in the original data.

To prove the effectiveness of Trio-based solution, we conduct a group of experiments for comparison. We attach the reference pair on a U-shape carton board (Fig. 12 (b)), and move the board along the vertical direction (*i.e.*, along the x-axis) above the target tag. As the purple line shown in Fig. 10, RSS stream of the target tag has a distinct decrease. Note that when applying AMPD we separate RSS streams into 0.2s windows. Therefore, we could get multiple valleys (*aka*, nadirs), as marked in red circles in Fig. 10. To eliminate the *fake nadirs*, *i.e.*, the identified nadir is only a local minimum RSS value but not the real one corresponding to the tag location, we compare the detected valleys with an empirical

threshold. We involve the valley (σ_{max}) which exceeds the threshold and its timestamp to determine the target location with respect to the reference pair (manipulator). On the other hand, Fig. 10 also proves that the RSS decreases in the one-interfering-tag case and the empty U-shape board case (*i.e.*, no interfering tags are attached on board) are less distinguishable, demonstrating the effectiveness and robustness of proposed Trio-based method.

3) Iterative Refining: We leverage the motion of the reference pair to iteratively refine the location of the target tag. Specifically, each pair of the motions (*e.g.*, moving horizontally and vertically) is an iteration. By aggregating these iterations, we can obtain a higher localization resolution.

The Class 1 Generation 2 standard [22] specifies that an RFID reader talks to tags following the frame slotted ALOHA protocol. This means a tag chooses a random time slot to respond to the reader. Hence the responses from the target tag may not exist when the reference pair is right over the target tag. To mitigate this impact, we extend the valley position (σ_{max}) detected in Section IV-A2, and take $[\sigma_{max} - \varepsilon, \sigma_{max} + \varepsilon]$ as the candidate positions (*i.e.*, indexes correspond to the positions) of one individual movement, where ε is a predefined threshold. In an iteration, after acquiring the candidate positions in one dimension (for example, σ_{max} for x-axis), Trio moves along the other dimension while keeping its x-coordinate as σ_{max}. Thus, for one iteration, we derive a candidate 2D region. After the end of each iteration, reference pair conservatively moves towards the target tag (*i.e.*, along y-axis) by D and derives a new candidate region. Finally, we use the center of the overlapped regions as the estimated location of the target tag. The whole algorithm is detailed in Algorithm 1.

Algorithm 1: Iterative refining algorithm

Input: RSS_{X1}, RSS_{Z1}: two sets of time serial RSS data obtained from one pair of motions;
$i = 2; D = \lambda/4; N = 5$

Output: $(\tilde{x}, \tilde{z})$: the x and z coordinate of the target tag

```
[σ_X1, σ_Z1] = valleyDetection(RSS_X1, RSS_Z1);
C_1 = candidateRegion(σ_X1, σ_Z1, ε);
O ← C_1;
for i <= N do
    Move along Y-axis by D;
    [σ_Xi, σ_Zi] = valleyDetection(RSS_Xi, RSS_Zi);
    C_i = candidateRegion(σ_Xi, σ_Zi, ε);
    O = overlayRegion(O, C_i);
    i ← i + 1, D ← D/2
end for
(x̃, z̃) = center(O);
```

B. Trio-based relative localization

Besides acquiring the absolute locations of individual tags, Trio also supports relative localization of a group of tags, *i.e.*, determining their order in a 2D plane. A lot of applications can benefit from the knowledge of relative locations, such as automatically finding misplaced items in the library, store, or production line.

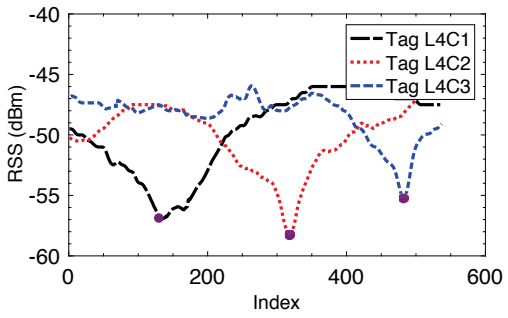

Fig. 11. Relative localization.

The basic idea of Trio-based relative localization is to move the reference pair over a set of tags, during which the RFID reader continuously interrogates those tags and obtains their IDs and RSS values. By analyzing the RSS trend of each tag and the temporal information of their valleys, Trio can obtain the spatial ordering among tags. Note the data preprocessing and valley detection algorithms are the same as Section IV-A.

We perform an experiment to validate above relative localization process. We deploy a 4×3 tag array on a carton, and move the reference pair across the fourth row. The results shown in Fig. 11 demonstrate the effectiveness of Trio. According to the sequential relationship of detected decreases (marked with purple circles) in Fig. 11, we can easily find the horizontal order of three tags in the fourth row.

V. Implementation and Evaluation

We implement a prototype of Trio and evaluate its performance through extensive experiments.

Hardware: The prototype of Trio is mainly built with a COTS RFID reader, Impinj R220. One directional antenna (Laird A9028, with gain of 8dbi) is mounted on the ceiling to interrogate tags on the table. The whole system works on the frequency of 922.38 MHz. The reader continuously interrogates tags and collects their IDs and RSS values. As shown in Fig. 12(a), we adopt seven different types of passive tags: 'Square', 'Short', 'Squiggle', 'Doc', 'Spider-360', 'BAT', and 'Impinj E41B'. They are mainstream labeling tags on the market. It is worth noting that these tags are with different sizes and antenna designs, demonstrating different radiation and anti-interference characteristics. The results show the generality of our method.

Software: The software of Trio is implemented using C#, which adopts the Low-Level Reader Protocol (LLRP, specified by EPCglobal in its EPC C1G2 standard) to communicate with the reader. The software runs on a PC with an Intel Core i7-4600U 2.10GHz CPU and 8GB RAM.

A. Setup and Parameter Selection

1) Antenna orientation of the reference pair: As shown in Fig. 2(a), the tag antenna is not symmetrical along its short edge. According to the direction to which the IC feed loop faces, we have two layout options, *i.e.*, in the same or opposite

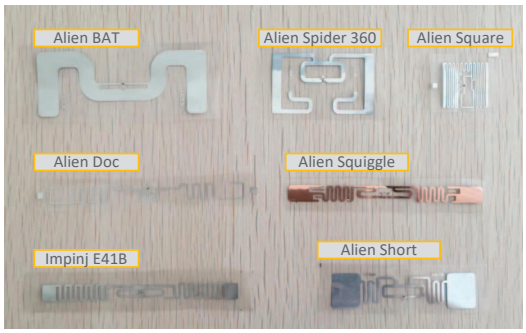

(a) Various tags adopted in the implementation

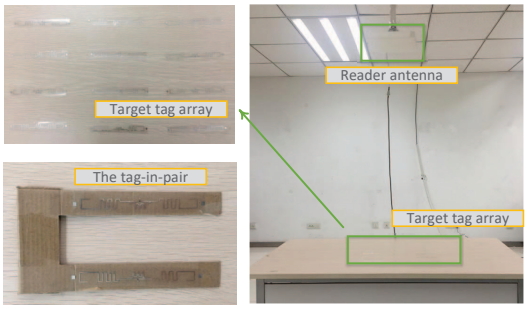

(b) Reference pair and target tag array

Fig. 12. Experiment setup

directions, when two tags are deployed in parallel. To test the impact of antenna direction on mutual coupling, we conduct a group of experiments. We put the target tag on the table, and move another tag (behaving as the interfering tag) above it. During above procedure, we collect the RSS sequence of the target tag. Fig. 13 compares the maximum RSS decreases when two tags are in the same and opposite directions. The results indicate that, for most kinds of tags involved in this experiment, the interference is more significant when two tags are in the opposite direction. Specifically, the RSS of Spider-360 tag experiences 20 dBm decrease in this case, while the standard deviation proves the interference is stable. Such a large change can greatly facilitate the location estimation. On the other hand, for Doc tag, it achieves the significant decrease in the same direction. To eliminate above potential impact, in Trio we deploy two interfering tags in opposite directions. By doing so, the target tag will always experience joint influence induced by the reference pair, no matter what orientation of the target tag itself is. This also proves the necessity of proposed two-interfering-tags solution.

2) Distance interval within the reference pair: Another deployment issue deserves attention is the distance between two interfering tags. If the distance interval is small, the mutual coupling will lead the decrease of the scattering power of the reference pair, which will further weaken its influence to the target tag. On the contrary, according to Fig. 8, the influence is more obvious when the reference pair is closer to the target tag. Considering the scenario of dense deployment of target tags and the requirement of localization accuracy, small distance interval is a good choice. To further determine the appropriate interval, we perform experiments with different distance intervals. We vary the interval within the reference pair from 1 cm to 10 cm, move it across a target tag, and estimate the maximum RSS decrease of the target tag. The results are shown in Fig. 14. The target tag achieves the maximum RSS decrease at the interval of 5 cm. As the distance increases or decreases, the influence attenuates gradually. Fig. 15 further demonstrates the RSS trends. In particular, the decrease is slight when the distance is 2 cm. Further, there is a 'W'-shape variation at the distance of 10 cm. This is because the interval is too large so that the influence from the reference pair is separated in the time domain. Synthetically considering above experimental results, we set the default interval within the reference pair as 5.5 cm. With such a setup, two tags in the reference pair locate at the boundary area between the near-field and far-field region of each other's electromagnetic field, where mutual coupling takes not obvious effect within the reference pair, while the essential influence to the target tag can be still guaranteed.

B. Performance of Absolute Localization

We investigate the performance of Trio-based absolute localization.

1) Overall performance: When the reference pair moves, we determine the target tag's 2D location as the location where the maximum RSS decrease appears. The location error is defined as the difference between the computed location and the real one. This group of experiments is conducted in a typical office building, where the experimental areas are surrounded with desks, chairs, and other facilities. The reference pair starts at a random position 0.3 m away from the target tag. The reader's transmitting power is set to 30 dBm, and the communication frequency is 922.38 MHz. Each experiment is repeated 30 times. We compare the localization accuracy of different tags and plot the result in Fig. 16. Recall that Trio leverages the interference among tags for localization. Apparently different tags have different anti-interference characteristics because of the antenna designs. We find that Trio achieves high accuracy when using 'Short', 'Squiggle', 'Doc', and 'Impinj E41B' tags. The corresponding location errors are about 0.75 ± 0.5 cm, 0.5 ± 0.25 cm, 1.1 ± 0.5 cm, 0.5 ± 0.25 cm, respectively. Trio can achieve sub-centimeter localization using these four main stream tags. The location errors exceed 2 cm when using the 'BAT' tag. This is because a BAT tag only experiences about a 4.5 dBm RSS decrease when the reference pair is around. Hence, it is difficult to correlate the Trio phenomenon with the location. We recommend that BAT tags are not suitable for Trio-based localization.

2) Angle tolerance: Ideally, Trio leverages the coupling between two tags that are deployed in parallel. In practice, the angle between two interfering tags may not keep an absolute parallel deployment. In this part, we choose Impinj E41B tag to evaluate the impact of the angle between reference pair and the target tag. We first estimate the influence in terms of RSS as this angle changes. Fig. 17(a) shows the maximum RSS decreases. The results reveal that the largest

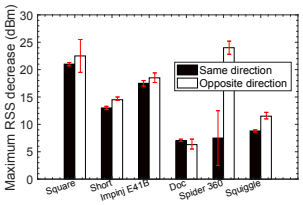

Fig. 13. Impact of tag antenna orientation.

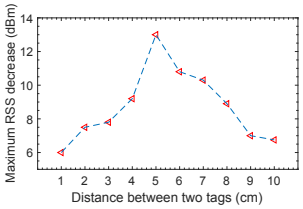

Fig. 14. Impact of interval within reference pair.

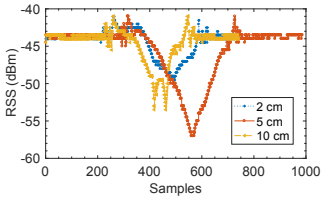

Fig. 15. Target tag RSS variation when interval within reference pair changes.

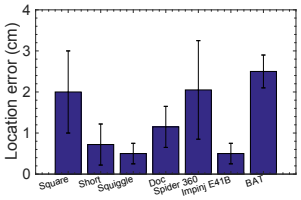

Fig. 16. Accuracy of absolute localization.

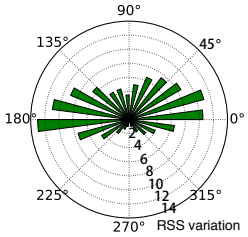

(a) RSS decrease at each angle

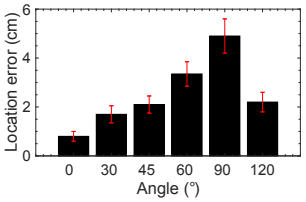

(b) Localization accuracy

Fig. 17. Angle tolerance of Trio-based absolute localization.

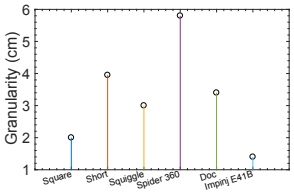

Fig. 18. Granularity distance of different target tags

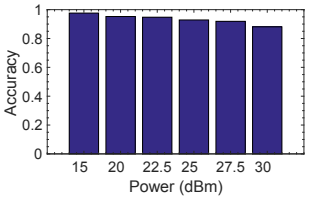

Fig. 19. Ordering accuracy vs. power

drop happens when tags are parallel (*i.e.*, 0° and 180°) to each other, indicating the maximum interference. On the other hand, the smallest drop appears when tags are perpendicular (*i.e.*, 90°). We further test the localization accuracy. We perform the localization algorithm 30 times at each angle. Fig. 17(b) plots the location errors. As expected, the error gradually increases when enlarging the angle and the error reaches its maximum value at the angle of 90°. When the angle is less than 45°, the average error is 1.9 cm, demonstrating an acceptable accuracy. Since the coupling effect is most effective when tags are parallel, we recommend such a deployment for real applications which demand high accuracy.

C. Performance of relative localization

1) Granularity distance among target tags: When determining the order among tags, it is worth to consider the distance between adjacent target tags. First, this distance should not be too short, otherwise the mutual coupling between target tags themselves would make them hard to be identified. Second, a short distance might also have implicit influence that makes the sequence of RSS troughs ambiguous in the time domain. Thus, we investigate the minimum distance (*i.e.*, the granularity) between target tags that Trio still supports the order deduction. The system parameters are set by default. In addition, we let the reference pair moves at the same speed. We increase the distance with a step length of 0.5 cm to test the granularity. Fig. 18 shows the results of using different tags as the targets. As aforementioned, these tags have different antenna designs (including the antenna size, materials, and structures). Thus, they demonstrate various granularities. For example, 'Spider 360' tag (5 cm × 3 cm) achieves good performance when the distance exceeds 6 cm. Both the 'Square' and 'Impinj E41B' tags can support order acquisition even they are deployed densely (closer than 2 cm). Above results provide suggestions of tag selection for various applications.

2) Order accuracy vs. power: In this set of experiments, we focus on the order accuracy of relative localization. We deploy a 4×3 Doc tag array as shown in Fig. 12(b), move the reference pair four centimeters above the tag array, and leverage the time-domain information to determine the appearance order of RSS valleys. The default distance between adjacent tags in the array is 6 cm. We vary the transmitting power of the reader antenna from 15 dBm to 30 dBm, and keep other settings consistent with aforementioned experiments. The reference pair is moved along each row and column. Each experiment is repeated 30 times. The average ordering accuracy is plotted in Fig. 19. When the reader's power is 30 dBm (the allowed maximum value), the accuracy is around 98%. The accuracy gradually decreases when reducing the power, and reaches around 88% when the power becomes 15 dBm. This result can be explained by the fact that the scattered energy of the reference pair is harvested from the reader. If the reader transmitting power is low, the interference that the target tag experiences due to the reference pair will be weakened, which reduces the accuracy of order deduction.

VI. Related Work

Prior localization methods in the literature can be divided into two categories: computer vision based and RF-signal based methods.

Computer vision based solutions [3], [4] rely on cameras/infrared sensors as well as planning and controlling algorithms. They usually require dedicated pre-training processes to identify a desired target. Since their real-world sensing is mostly based on visual information, such as images or videos, those works may fail in recognizing objects with similar colors or shapes. Meanwhile, those approaches are sensitive to the change of lighting and background. Also those works cannot operate in non-line-of-sight scenarios.

RF-based methods [9], [23], [24], [25] become attractive since they release the line-of-sight constraint. However, most wireless signal based methods do not support recognizing specific objects directly. It might be a solution if attaching existing wireless devices with the ability of reporting identities, *e.g.*, cellphones, to target objects. Hence reducing the device cost is an essential requirement. In comparison with prior works, Trio naturally solves the object recognition problem by leveraging the identification function of RFID tags (*i.e.*, acquiring the unique IDs from the tags).

Several works [9], [24], [26], [27] have been proposed for indoor localization using RFID tags. Tagoram [9] utilizes moving tags to simulate the inverse SAR antennas and pinpoints a tag with the accuracy of a few centimeters. RF-IDraw [24] tracks a moving tag and deduces its trajectory in the air. However, the strong assumption of target tag movements has severely limited the implementation of those works in practice. In addition, they both require closely-spaced and rigid configuration of reader antenna arrays. Other approaches, for example, PintIt [7] utilizes SDR to exploit multipath profiles as fingerprints of tags' spatial locations and accurately locates RFID tags. Nonlinear Backscatter [26] utilizes second and higher-order harmonic signals to eliminate phase cycle ambiguity and enables 3D localization. However, these systems also suffer from several constraints, such as the requirement of reference tags as anchor nodes [7], dedicated devices [10], or modification of the hardware [26]. Compared to the above approaches, Trio provides an RF interference-based refined tag localization solution, which utilizes off-the-shelf RFID devices to accurately locate the target with $<$1 cm accuracy for several models of main stream tags.

VII. Conclusions

This paper presents Trio, an accurate RFID localization system for refined localization that is useful for many applications, *e.g.*, autonomous robots. Trio detects the object by identifying the attached tag and leverages RF interference of coupled tags to facilitate localizing the target. We implement a prototype of Trio using COTS UHF RFID devices and perform extensive experiments to evaluate its performance. The results demonstrate that Trio is fully compatible with existing industrial standard and exhibits high accuracy for both absolute and relative localization.

Acknowledgements

This work was supported by National Basic Research Program of China (973 Program) under Grant No.2015CB351705, NSFC Grant No.61572396, 61772413, 61672424, China 863 Grant 2013AA014601, and National Science and Technology Major Project of the Ministry of Science and Technology of China JZ-20150910. Chen Qian was supported by National Science Foundation Grants CNS-1701681 and CNS-1717948. Fu Xiao was supported by Nature Science Foundation of Jiangsu for Distinguished Young Scientist under Grant BK20170039. Chen Qian is the corresponding author.

References

[1] C. C. Kemp, A. Edsinger, and E. Torres-Jara, "Challenges for Robot Manipulation in Human Environments," *IEEE Robotics and Automation Magazine*, vol. 14, no. 1, p. 20, 2007.

[2] R. T. Chin and C. R. Dyer, "Model-based Recognition in Robot Vision," *ACM Computing Surveys (CSUR)*, vol. 18, no. 1, pp. 67–108, 1986.

[3] R. A. Knepper, T. Layton, J. Romanishin, and D. Rus, "Ikeabot: An Autonomous Multi-robot Coordinated Furniture Assembly System," in *IEEE ICRA*, 2013.

[4] S. Nirjon and J. A. Stankovic, "Kinsight: Localizing and Tracking Household Objects using Depth-camera Sensors," in *IEEE DCOSS*, 2012.

[5] J. Xiong and K. Jamieson, "ArrayTrack: A Fine-grained Indoor Location System," in *USENIX NSDI*, 2013.

[6] N. Kothari, B. Kannan, E. D. Glasgwow, and M. B. Dias, "Robust Indoor Localization on a Commercial Smart Phone," *Procedia Computer Science*, vol. 10, pp. 1114–1120, 2012.

[7] J. Wang and D. Katabi, "Dude, Where's My Card?: RFID Positioning That Works with Multipath and Non-line of Sight," in *ACM SIGCOMM*, 2013.

[8] L. Shangguan, z. Zhou, and K. Jamieson, "Enabling Gesture-based Interactions With Object," in *ACM MobiSys*, 2017.

[9] L. Yang, Y. Chen, X. yang Li, C. Xiao, M. Li, and Y. Liu, "Tagoram: Real-time Tracking of Mobile RFID Tags to High Precision Using COTS Devices," in *ACM MobiCom*, 2014.

[10] J. Wang, F. Adib, R. Knepper, D. Katabi, and D. Rus, "RF-compass: Robot Object Manipulation Using RFIDs," in *ACM MobiCom*, 2013.

[11] J. Han, H. Ding, C. Qian, W. Xi, Z. Wang, Z. Jiang, L. Shangguan, and J. Zhao, "CBID: A Customer Behavior Identification System using Passive Tags," *IEEE/ACM Transactions on Networking*, vol. 24, no. 5, pp. 2885–2898, 2016.

[12] L. Xie, J. Sun, Q. Cai, C. Wang, J. Wu, and S. Lu, "Tell Me What I See: Recognize RFID Tagged Objects in Augmented Reality Systems," in *ACM UbiComp*, 2016.

[13] H. Ding, J. Han, L. Shangguan, W. Xi, Z. Jiang, Z. Yang, Z. Zhou, P. Yang, and J. Zhao, "A Platform for Free-weight Exercise Monitoring with RFIDs," *IEEE Transactions on Mobile Computing*, vol. 16, no. 12, pp. 3279–3293, 2017.

[14] H. Ding, C. Qian, J. Han, G. Wang, Z. Jiang, J. Zhao, and W. Xi, "Device-free Detection of Approach and Departure Behaviors using Backscatter Communication," in *ACM UbiComp*, 2016.

[15] Y. Bu, L. Xie, J. Liu, B. He, Y. Gong, and S. Lu, "3-Dimensional Reconstruction on Tagged Packages via RFID Systems," in *Proceedings of IEEE SECON*, 2017.

[16] Q. Chen, N. Hoilun, L. Yunhao, and N. M. Lionel, "Cardinality Estimation for Large-Scale RFID Systems," *IEEE Transactions on Parallel and Distributed Systems*, vol. 22, no. 9, pp. 1441–1454, 2011.

[17] D. Dobkin, *The RF in RFID: Passive UHF RFID in Practice*. Elsevier Inc, 2008.

[18] S. A. Schelkunoff and H. T. Friis, *Antennas: theory and practice*. Wiley New York, 1952, vol. 639.

[19] S. J. Orfanidis, *Electromagnetic Waves and Antennas*. Rutgers University New Brunswick, NJ, 2002.

[20] T. Liu, L. Yang, Q. Lin, Y. Guo, and Y. Liu, "Anchor-free backscatter positioning for rfid tags with high accuracy," in *IEEE INFOCOM*, 2014.

[21] F. Scholkmann, J. Boss, and M. Wolf, "An Efficient Algorithm for Automatic Peak Detection in Noisy Periodic and Quasi-periodic Signals," *Algorithms*, vol. 5, no. 4, pp. 588–603, 2012.

[22] EPCglobal, *Specification for RFID Air Interface EPC: Radio-Frequency Identity Protocols Class-1 Generation-2 UHF RFID Protocol for Communications at 860 MHz-960 MHz*, 2008.

[23] J. Han, C. Qian, X. Wang, D. Ma, J. Zhao, W. Xi, Z. Jiang, and Z. Wang, "Twins: Device-free Object Tracking using Passive Tags," *IEEE/ACM Transactions on Networking*, vol. 24, no. 3, pp. 1605–1617, 2016.

[24] J. Wang, D. Vasisht, and D. Katabi, "RF-IDraw: Virtual Touch Screen in the Air using RF Signals," in *ACM SIGCOMM*, 2014.

[25] X. Zheng, Z. Cao, J. Wang, Y. He, and Y. Liu, "ZiSense: Towards Interference Resilient Duty Cycling in Wireless Sensor Networks," in *ACM SenSys*, 2014.

[26] Y. Ma, X. Hui, and E. C. Kan, "3D Real-time Indoor Localization via Broadband Nonlinear Backscatter in Passive Devices with Centimeter Precision," in *ACM MobiCom*, 2016.

[27] F. Xiao, Z. Wang, N. Ye, R. Wang, and X.-Y. Li, "One More Tag Enables Fine-Grained RFID Localization and Tracking," *IEEE/ACM Transactions on Networking*, vol. PP, no. 99, pp. 1–14, 2017.